The Effect of MOSFET Second-Order Nonlinearity on Active Inductor-Based Oscillators

Ler Chun Lee[1, 2], Abu Khari bin A'ain[1] and Albert Victor Kordesch[2]
[1] Faculty of Electrical Engineering, University of Technology Malaysia, Skudai, Johor, Malaysia
[2] Department Device Modeling, Silterra Malaysia Sdn. Bhd., Kulim, Kedah, Malaysia
Email: chunlee_ler@silterra.com, abu@fke.utm.my, al_kordesch@silterra.com

Abstract— **Second-order nonlinearity of the MOSFET has significant impact on active inductor (AI) based oscillators, regardless of whether they are single-ended or differential. By using Taylor series expansion, this paper shows that second-order nonlinearity of the MOSFET will cause a shift in the DC biasing of an AI-based oscillator, depending on oscillation amplitude. The DC bias shift results in a change of the transistor transconductance and parasitic components from their original value, which will affect the oscillator resonance frequency. This explains why a small-signal S-parameter simulation is not sufficient to accurately predict the oscillation frequency and tuning range of AI-based oscillators, even at moderate oscillation amplitudes.**

I. INTRODUCTION

Due to the high demand from the market, different wireless communication services and applications operate at different available frequency bands. Examples are cellular networks and wireless local area networks (WLAN) that include 802.11a, 802.11b, 802.11g, HiperLAN1, HiperLAN2, and Bluetooth. To further reduce the device size and production cost of the wireless communication devices, a compact and power-efficient device that can support various wireless standards that operate at different frequency bands is desired.

One of the difficulties for the multistandard transceiver realization is design an oscillator with large tuning range, which can cover different frequency bands of interest. Although multiple oscillators each with a narrow tuning range can simply solve the problem, this is not cost and power effective. The AI-based oscillator becomes a very attractive candidate due to its large tuning range. Different designs of AI-based oscillators have been proposed in the literature [1-4].

Since oscillators usually require large oscillation amplitude for minimum phase noise, the behavior of the active inductor in an AI-based oscillator cannot be approximated by small-signal analysis and a static DC operating point. Due to the nonlinearity of the MOSFET, tranconductance (g_m), parasitic capacitance and conductance of the transistor will vary according to oscillation amplitude. Unfortunately, inductance of the active inductor greatly depends on g_m and parasitic capacitance of the transistor.

Previous circuit linearity analyses mostly focus on third-order nonlinearity of the MOSFET since it is very important to determine the 1dB compression point and the third-order intercept point (IIP3) of the circuit [5-6]. However, in an AI-based oscillator, second-order MOSFET nonlinearity also becomes one of the main contributors to the nonlinearity, even at moderate oscillation amplitude. It affects the AI-based oscillator by shifting the DC biasing of the MOSFET from its original design value, thus changing the resonance frequency of AI-based oscillator. The effect becomes even more obvious when the MOSFET is biased at low gate overdrive voltage for low-power application.

Due to its simplicity, Taylor series expansion has been adopted in this paper for active inductor linearity analysis. More accurate results can be obtained by using Volterra series expansion but it involves very complex mathematical derivation. However, good approximations for the AI-based oscillator large-signal behavior can be obtained by considering MOSFET second and third-order nonlinearity using Taylor series expansion, much better than small-signal S-parameter simulation.

The paper is organized as follows: Section II discuss the effect of the MOSFET second-order nonlinearity on the AI-based oscillator. Section III adopts the design of AI-based oscillator in [1] with some modifications for verification. Calculation results are compared to HSPICE transient and small-signal S-parameter simulation results. Section IV discusses calculation and simulation results from Section III. Finally, section V concludes the paper.

II. MOSFET SECOND-ORDER NONLINEARITY

The value of drain current, I_{ds} at certain small-signal v_{sig} around V_{GS} , where V_{DS} is fixed, can be represented by a Taylor series expansion shown below [5]:

$$I_{ds}(V_{GS}+v_{sig}) = c_0 + c_1 v_{sig} + c_2 v_{sig}^2 + \ldots + c_n v_{sig}^n \quad (1)$$

where $c_n = \frac{1}{n!}\frac{\partial^n I_{DS}}{\partial V_{GS}^n}$.

1-4244-1435-0/07/$25.00©2007 IEEE

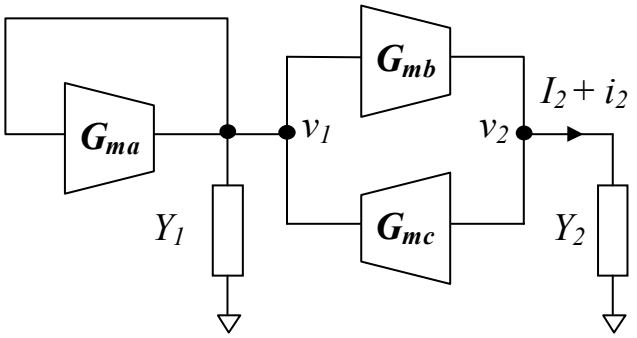

Figure 1. Simplified block diagram of AI-based oscillator

By considering only up to second-order nonlinearity and assuming $v_{sig} = A\cos\theta$, the total DC drain current can be found from (1),

$$I_{DS}(V_{GS} + v_{sig}) \approx c_0 + \frac{c_2 A^2}{2} \tag{2}$$

This equation is similar in form to the well known MOSFET saturation drain current formula,

$$I_{DS}(V_{od} + v_{sig}) \approx \frac{\beta}{2}(V_{od}^2 + \frac{A^2}{2}) \tag{3}$$

where $V_{od} = V_{GS} - V_{TH}$ and $\beta = \mu_e C_{OX} W / L$. μ_e, C_{OX}, W, and L are electron mobility, gate oxide capacitance per unit area, and transistor width and length, respectively.

From (2) and (3) we conclude that MOSFET DC drain current not only depends on DC gate to source voltage, but it is also a function of input signal amplitude.

Figure 1 shows the simplified block diagram for an AI-based oscillator, where transconductor G_{ma} provides the necessary negative resistance to start the oscillation, and transconductor G_{mb} and G_{mc} form the gyrator active inductor. To simplify the analysis, only nonlinear behavior of transconductance is considered and it's V-I relationship can be represented by the Taylor series expansion shown in (2). Assuming $v_1 = A\cos\theta$ during steady state oscillation, the DC voltage of v_2 is

$$V_2 = I_2 / real(Y_2) \tag{4}$$

where $I_2 = c_0 + c_2 A^2 / 2$ if the current is not limited by the current source or other devices. According to (4), If the transconductor G_{mc} is designed with a transistor whose gate or source voltage is defined by V_2, the gate or source voltage will vary from its original value, depending on the amplitude of v_2. The transistor's gate or source DC voltage shift causes the effective transconductance of G_{mc} to be changed and this will further vary the resonance frequency of the AI-based oscillator. A similar case also applies in the transconductors G_{ma} and G_{mb}.

In most cases the DC current flow in the active inductor is fixed by a current source. To gain further insight to the case with a current source, assume a common-source transistor is used to construct the inverse transconductor in a gyrator circuit, where its DC current is fixed by an ideal current source, I_{DC}. When the oscillation amplitude, $A = 0$,

$$I_{DC} = I_{DS} = \frac{\beta}{2} V_{od1}^2 \tag{5}$$

where V_{od1} is the DC overdrive voltage at $A = 0$.

When the AI-based oscillator starts to oscillate, the MOSFET second-order nonlinearity will generate excess DC current in the circuit. According to Kirchoff's Current Law,

$$I_{DC} \approx \frac{\beta}{2}(V_{od2}^2 + \frac{A^2}{2}) \tag{6}$$

where V_{od2} is DC overdrive voltage at steady state oscillation. Comparing (5) and (6), since I_{DC} is fixed, it is straight forward to show that $V_{od2} < V_{od1}$. The DC overdrive voltage is decreased from its original value, which is a function of oscillation amplitude. The effect is obvious especially if the MOSFET is biased at low overdrive voltage for low-power application.

III. VERIFICATION

To verify the derivation in the previous section, an AI-based oscillator is designed based on a current-controlled oscillator (CCO) proposed in [1] using Silterra's 0.18μm CMOS BSIM 3v3 RF model with some modifications. Since NMOS is a more popular choice than PMOS transistor in active inductor design, the CCO in this paper adopts an active inductor that is designed using NMOS transistors. The circuit diagram of the CCO is shown in Figure 2. HSPICE transient and small-signal S-parameter simulation is used for comparison and verification. All the required parameters of the MOSFET are extracted from the model, including Taylor series expansion coefficients for the drain current, high frequency parasitic capacitance and conductance. As mentioned before, only the nonlinear behavior of the transconductance of the MOSFET is considered.

Figure 3 shows the single-ended active inductor used in the CCO. Its input admittance can be derived using small-signal analysis, as show below

$$Y_{in} = sC_1 + g_1 + g_{m2} + y_{ds2} + \frac{(g_{m2} + y_{ds2})(g_{m1} - y_{ds2})}{y_{ds2} + sC_2 + g_2}$$

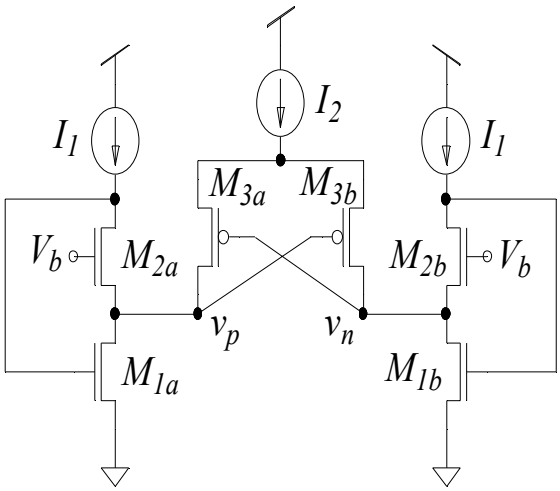

Figure 2. Circuit diagram of the CCO used for verification

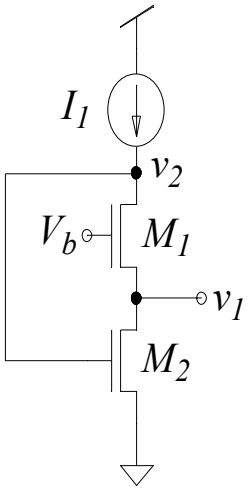

Figure 3. Active inductor circuit diagram

$$C_{eff} = C_1 + C_{db2} + C_{gd1} \qquad L_{eff} \approx \frac{C_2 + C_{db2} + C_{gd1}}{g_{m1} g_{m2}}$$

$$w_R = 1/\sqrt{C_{eff} L_{eff}} \tag{7}$$

where $y_{ds2} = g_{ds2} + sC_{db}$, C_{db} , C_{gd} , g_m and g_{ds} represent drain-bulk capacitance, gate-drain capacitance, transconductance and output conductance of corresponding transistors. C_1 , C_2 , and g_1 , g_2 represent parasitic capacitance and conductance at node v_1 and v_2, respectively. w_R is the self-resonance frequency of the active inductor.

To give flexible control of oscillation amplitude while keeping other transistor parameters constant, a variable tuning capacitor C_{ext} has been inserted between node v_p and v_n in the CCO. The effect of C_{ext} on the resonance frequency of CCO can be included in C_{eff} . The CCO is simulated using HSPICE transient simulation and the time-average DC gate-source voltage is extracted from the transient simulation by using the following formula,

$$V_{GS} = \frac{1}{T}\int_0^T V_{gs}(t)dt \tag{8}$$

where T is period of the signal. Figure 4 shows the time-average DC gate-source voltage of M_1 for different values of v_{gs1} oscillation amplitude. As expected, larger oscillation amplitude will reduce transistor DC overdrive voltage by generating excess DC current due to the second-order nonlinearity of the transistor.

Table I shows the comparison between HSPICE transient simulation and calculation for four different v_{gs1} oscillation amplitudes. Calculation is based on (3), where the value of Taylor series expansion coefficients is obtained at the steady-state time-average M1 DC gate-source voltage. From Table I, the error between calculation and transient simulation result is not more than 10% although a simple second order Taylor series expansion is used.

Figure 5 shows a comparison between the various simulated and calculated CCO resonance frequencies, as a function of tuning capacitance C_{ext} . The small-signal S-parameter simulation can not predict resonance frequency of AI-based oscillator very well because it does not include the nonlinearity effect of the MOSFET. Furthermore, small-signal S-parameter simulation assumes the circuit has a static DC operating point which is independent of the incoming signal amplitude. Figure 5 also shows that a calculation which only includes MOSFET third-order nonlinearity does not predict behavior of AI-based oscillator very well, especially at large oscillation amplitude (or small C_{ext} value).

TABLE I. COMPARISON BETWEEN CALCULATION AND TRANSIENT SIMULATION FOR v_{gs1} OSCILLATION AMPLITUDE

Steady-state V_{GS1}(mV)	***Oscillation Amplitude of v_{gs1}***	
	Calculation (mV)	***Transient Simulation (mV)***
702.6	366.0	393.3
725.8	345.4	350.3
744.3	319.7	311.0
762.5	277.7	259.4

IV. DISCUSSION

Unlike spiral (or passive) inductor-based LC oscillators, AI-based oscillators show a tradeoff between oscillation amplitude and frequency, due to MOSFET nonlinearity. Higher oscillation amplitude will significantly decrease transconductance of the transistor and thus reduce the oscillation frequency, and vice-versa. The tradeoff between

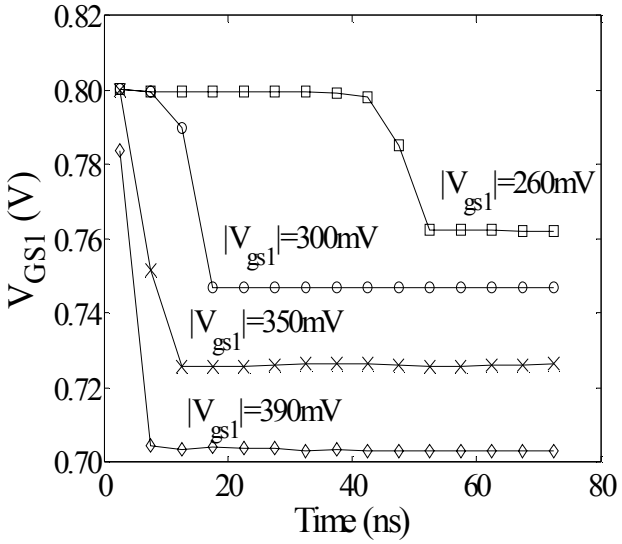

Figure 4. Time-average DC gate-source voltage of M1 versus time. After reaching steady state, the average VGS is seen to depend on oscillation amplitude |Vgs|. Four different amplitudes are shown.

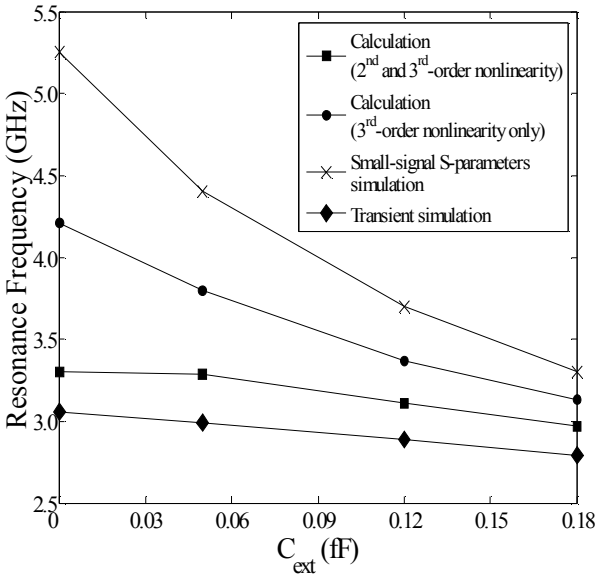

Figure 5. Comparison of various simulated and calculated CCO resonance frequencies, as a function of tuning capacitance C_{ext}.

oscillation amplitude and frequency also implies that the tuning range of AI-based oscillators will be decreased. It can be observed from Figure 5, for the same tuning range of C_{ext}, small-signal S-parameter simulation shows a higher tuning range compared to transient simulation. Again, nonlinearity is responsible for the limited tuning range in the transient simulation.

Oscillation amplitude of the CCO will increase when smaller C_{ext} is used. However, larger oscillation amplitude will decrease transconductance of transistor and increase inductance of active inductor. The resonance frequency of CCO is almost constant since inductance of active inductor is inversely proportional to C_{ext}.

From the previous discussion, the AI-based oscillator shows strong correlation between tuning range, oscillation amplitude and frequency. The correlation can be reduced if transistors have better linearity. This can be achieved by biasing the transistor at high gate overdrive voltage but at the cost of higher power dissipation.

Unfortunately, differential AI-based oscillators that are usually expected to have better rejection of the second-order nonlinearity also experience the same DC operating point shifting effect as single-ended AI-based oscillators. Although the differential output signal of differential AI-based oscillators only contain odd-harmonic signals, the frequency and amplitude of odd-harmonic signals are also determined by DC parameters of transistor, which include transconductance. The effect of DC operating point shifting can not be canceled out like even–order harmonics by using a differential circuit.

V. CONCLUSION

This paper presented the effect of MOSFET second-order nonlinearity on AI-based oscillators. It is mainly responsible for the shifting of the DC operating point, which is a function of oscillation amplitude. The effect can not be ignored for AI-based oscillators, regardless whether they are single-ended or differential. By using a Taylor series expansion for transistor drain current up to third order, the calculated resonance frequency of a CCO shows very good agreement with the transient simulation result.

Unlike passive inductor-based LC oscillators, AI-based oscillators show a strong correlation between tuning range, oscillation amplitude and frequency. MOSFET nonlinearity effects need to be taken into consideration when an AI-based oscillator with large oscillation amplitude and higher resonance frequency is desired.

REFERENCES

[1] Y. Wu, M. Ismail, and H. Olsson, "CMOS VHF/RF CCO based on active inductors," *IET Electronic Letters*, vol. 37, no. 8, pp. 472-473, April 2001.

[2] R. Mukhopadhyay, Y. Park, P. Sen, N. Srirattana, J. Laskar, "Reconfigurable RFICs in Si-based technologies for a compact intelligent RF front-end," *IEEE Trans. Microw. Theory Tech.*, vol. 53, no. 1, pp. 81-93, Jan. 2005.

[3] Liang-Hung Lu, Hsieh-Hung Hsieh, and Yu-Te Liao, "A Wide Tuning-Range CMOS VCO With a Differential Tunable Active Inductor," *IEEE Trans. Microw. Theory Tech.*, vol. 54, no. 9, pp. 3462-3468, Sep. 2006.

[4] Joy Laskar, Rajarshi Mukhopadhyay, and Chang-Ho Lee, "Active Inductor-Based Oscillator: A Promising Candidate for Low-Cost Low-Power Multi-Standard Signal Generation," *IEEE Radio and Wireless Symposium*, pp. 31-34, Jan. 2007.

[5] T. Soorapanth and Thomas H. Lee, "RF linearity of short-channel MOSFETs," *Proceedings of 1st International Workshop on Design of Mixed-mode IC and Applications*, pp. 81-84, 1997.

[6] Q. Li and J. S. Yuan, "Linearity analysis and design optimisation for 0.18um CMOS RF mixer," *IEE Proc.-Circuits Devices Syst.*, vol. 149, no. 2,, pp. 112-118, April 2002.